Determination of orbital elements of 138846 2000 VJ61 via the method of Gauss

Team #1: The Natural Disasteroids

Jessica Dong, Lauren Fossel, Hagan Hensley

Location: New Mexico Institute of Mining and Technology, Etscorn Observatory

Date: July 22, 2017

ABSTRACT:

The primary objective in this project was to calculate the orbit of the asteroid 2000 VJ61 by utilizing the Method of Gauss. The orbital elements include the semi-major axis of the orbit, the eccentricity of the ellipse, the inclination with respect to the ecliptic, the longitude of the ascending node, the argument of perihelion, and the true anomaly. To collect the data required to perform this method of orbit determination, our team took weekly images of the asteroid at Etscorn Observatory with a 14-inch Schmidt-Cassegrain telescope. These images were then processed through LSPR code written by each team

member to obtain the right-ascension and declination for each set of images. The numerous sets of data for each successful observation were then passed into Python code written by each team member that employed the Method of Gauss. The elements were then corrected using differential correction. After examining our results and comparing them to values calculated by JPL, we can conclude that our orbit determination was successful in returning reasonable orbital elements.

INTRODUCTION:

Our goal in this project was to, based on observations, determine the orbit of 2000 VJ61 in terms of its orbital elements. The orbital elements include the semi-major axis of the orbit, the eccentricity of the ellipse, the inclination with respect to the ecliptic, the longitude of the ascending node, the argument of perihelion, and the true anomaly. To determine the orbital elements, we performed LSPR on the data to find the right ascension and declination of the asteroid for each observation. We then used the Method of Gauss to calculate the orbital elements. For near-Earth asteroids such as 2000 VJ61, determining and constantly updating the orbital elements precisely is a relevant goal in order to ensure that any perturbations from the Keplerian orbit that lead to the asteroid being nudged onto a course towards Earth are noticed.

MATERIALS AND METHODS:

The telescope used to observe asteroid 2000 VJ61 was a 14-inch Schmidt-Cassegrain telescope at Etscorn Observatory, New Mexico Tech, Socorro, New Mexico; latitude 34° 04’ 21.46’’ N, longitude 106° 54’ 51.8’’ W, elevation 1429 m. TheSkyX software was used to control the telescope, identify the asteroid’s location in the field of view, and select reference stars for

image analysis. CCDSoft was used to reduce images, blink multiple images in order to precisely identify the location of the asteroid in each image, identify the approximate pixel coordinates of the reference stars in each image, and select the clearest, sharpest image on which to perform astrometry.

During each two-hour observing slot, when the weather was clear, observations were taken in three sets of five consecutive images, each one with a 60 second exposure. The CCD was always kept cooled to a temperature of -10° C. The sets were separated by approximately 15 minutes from each other to ensure that the asteroid moved sufficiently between each set. Seeing was generally good, allowing the asteroid's position to be calculated with fairly low uncertainty in most images. In between sets, eleven dark and bias frames were taken for each successful night of observing. The camera's filter was set to clear in order to let in the most light, since 2000 VJ61 became very dim (approaching 17th magnitude) by mid July, at the end of the observing period. On cloudy nights when the asteroid was not visible, the two-hour observing slot was instead used to obtain data on the dependence of bias and dark frames on time and temperature, the analysis of which is detailed further in Appendix B.

To determine the asteroid's orbital elements based on its right ascension and declination on each night, the Method of Gauss was used. For each night, one image was selected to be used in the Method of Gauss. Going through each possible permutation of observations that maximizes the time between the first and last (observations 1, 2, 4, and 1, 3, 4), the Method of Gauss first uses the Scalar Equation of Lagrange to calculate an initial value for the asteroid's distance r_2 from the sun at the time of central observation. From this value, the scalar equations of range are used to estimate the range vectors ρ_1,ρ_2,ρ_3 from the Earth to the asteroid at the time of each observation, from which the position and velocity vectors of the asteroid can be estimated at the time of central observation. All initial values have now been calculated, so the

process of iteration can begin. In each iteration, the time of each observation is first corrected for light travel time based on each calculated range vector. Following this, the fourth-order f and g Taylor series are used to arrive at more accurate values for the range vectors from the scalar equations of range. Then the position and velocity vectors at the time of the central observation are recalculated, giving more accurate numbers than the previous iteration. This process is repeated until the position vector at the time of central observation appears to have converged, varying from one iteration to the next by less than 10^{-12} AU. The final position and velocity vectors of the asteroid are then converted into the six orbital elements.

After the orbital elements were determined, Hensley's Method of Gauss program automatically visualized the asteroid's orbit in the context of the rest of the solar system, showing how 2000 VJ61 has a fairly high eccentricity and comes within the Earth's orbit while at other times going almost all the way out to Jupiter. Fossel's Method of Gauss code has the option to switch between the f and g closed form functions and the fourth order f and g series.

DATA AND ANALYSIS:

List of observations:

Date and time (UT)	Asteroid RA and dec	RA, dec uncertainty	Observing conditions	Asteroid magnitude	Sky Brigh-tness (ADU)	Signal to noise ratio	Notes
2017/06/23 06:20:32	17h 27m 15.08s, -24° 44' 53.0''	0.28'' RA 0.19'' dec	Very good, but a lot of background noise in	14.6	70.46	32.86	Observation borrowed from Team 8

			pictures				
2017/06/29 07:53:17	17h 24m 45.40s, -19° 56’ 10.0’’	0.09’’ RA, 0.19’’ dec	Very good, completely clear	15.8	302.5	803.049	
2017/07/12 05:27:24	17h 24m 45.25s, -13° 43’ 10.8’’	0.27’’ RA, 0.19’’ dec	Mostly cloudy, poor seeing	16.3	442.7	226.267	Only 2 sets taken due to clouds
2017/07/15 04:23:37	17h 25m 32.53s, -12° 49’ 03.3’’	0.20’’ RA, 0.20’’ dec	Fair, mostly clear	16.7	175.3	221.111	

LSPR (least squares plate reduction) was used for astrometry in order to calculate the asteroid’s position in each image to within a fraction of an arcsecond based on the known positions of surrounding stars. The validity of the raw data was assessed by comparing the calculated ra and dec to the apparent position of the asteroid based on the background stars in Sky X. We also picked images to process in which the asteroid had the smallest diameter, so the best seeing.

Signal to noise ratio was calculated using the CCD equation, using the value of the median sky background in each annulus and assuming a read noise of 15 e^-, an A/D gain of 2 e^-/ADU, and a dark current of 0.11 ADU/pixel/second at a temperature of -10° C using the fit calculated in Appendix B.

Team members' calculated orbital elements and uncertainty:

Team member	a	e	I	Ω	ω	M
Fossel	2.212 AU +/- 0.009 AU	0.5722 +/- 0.002	18.803° +/- 0.05°	270.595° +/- 0.005°	280.030° +/- 0.03°	31.344° +/- 0.2°
Hensley	2.212 AU +/- 0.009 AU	0.572 +/- 0.002	18.804° +/- 0.05°	270.607° +/- 0.005°	280.02° +/- 0.03°	31.347° +/- 0.2°
Dong	2.235 AU +/-0.01 AU	0.576 +/-0.002	18.921° +/- 0.05°	270.596° +/-0.006°	280.076° +/- 0.03°	30.823° +/-0.3°

To determine the uncertainty on the orbital elements, the uncertainty on the right ascension and declination for each observation were used to calculate new orbital elements.

Description of Orbital Elements:

- a is the semimajor axis of the ellipse, in AU.
- e is the eccentricity of the orbit. It represents the elongation of the ellipse. An eccentricity of 0 is a circle, and 1 is a parabolic orbit.

- I is the inclination of the orbit in degrees. It is the angle between the asteroid's orbital plane and the ecliptic.
- Ω is the longitude of the ascending node in degrees eastward. The ascending node is the place where the asteroid's orbital plane intersects the ecliptic plane, going from south to north. The longitude of the ascending node is the angle between the Vernal Equinox and the asteroid's ascending node.
- ω is the argument of perihelion measured in degrees eastward from the orbital plane of the asteroid. It is the angle between the ascending node and the asteroid's point of closest approach to the Sun (perihelion).
- M is the mean anomaly measured in degrees from the perihelion. The mean anomaly puts the asteroid at a specific spot in its orbit. It represents the angular position the asteroid would have if its orbit were circular around the center of its ellipse.

Prediction of other team's measured asteroid position:

	Other team's measured asteroid position:	Our predicted asteroid position:
Observation 2	RA: 17:25:24.62 Dec: -21:24:54.9	RA: 17:25:24.75 Dec: -21:25:12.1
Observation 3	RA: 17:24:11.00 Dec: -18:04:24.00	RA: 17:24:10.9 Dec: -18:03:54.9
Observation 4	RA: 17:24:00.84 Dec:-16:07:06.70	RA: 17:24:0.64 Dec: -16:06:33.1

The calculated orbital elements predict the other team's measured asteroid position fairly well. None of the predicted values differ more than around 30 arc seconds from the other team's measured asteroid position.

Results of differential correction:

	RMS before correction (arcsec)	RMS after correction (arcsec)
Fossel	75.1"	6.81"
Hensley	11.2"	6.70"
Dong*	75.1"	6.83"

*Note: These values were calculated through Fossel's differential correction code using Dong's r and rdot vectors.

Orbital elements according to JPL Horizons:

a	e	I	Ω	ω	M
2.1847 AU	.5630	18.678°	270.581°	280.480°	32.040°

Percent difference of calculated orbital elements from JPL Horizons orbital elements

	% difference for a	% difference for e	% difference for I	% difference for Ω	% difference for ω	% difference for M

Fossel	1.24%	1.62%	.667%	.00517%	.161%	2.20%
Hensley	1.22%	1.57%	.670%	.00961%	.164%	2.21%
Dong	2.28%	2.28%	1.29%	.00554%	.144%	3.87%

None of the calculated orbital elements agree within the uncertainty with the orbital elements generated from JPL Horizons, though none are more than a couple of percent off.

Based on the calculated orbital elements, 2000 VJ61 is an Apollo. 2000 VJ61 has a semimajor axis greater than 1 AU, and a minimum distance from the sun of .946 AU. These characteristics mean that 2000 VJ61 is an Apollo.

CONCLUSION:

We are fairly confident about our orbital elements for multiple reasons. The orbital elements between each team member were very similar, and they were also fairly similar to JPL. It makes sense that the JPL values differ from our values because the values in JPL were last calculated in June of 2013, and orbits of asteroids change. Also, the root mean square values after the differential corrections are only a few arc seconds, meaning that the calculated orbits closely matched our actual observations. We are not completely confident about our values because there is always error involved with taking and analyzing data. The sources of unavoidable error are the LSPR, and the inherent error in the telescope, mount, and CCD camera.

If we were to do this again, we would like to have more observations so that our differential correction was better and so that we wouldn't have to use the other team's data. We also would have thought ahead more in terms of the code, for example making the ephemeris

generation a large function to start with instead of printing out values. If colleagues wanted to replicate the project, we would recommend keeping close track of which photos are used for the astrometry, and having each team member perform each step of the process.

APPENDIX A: MPC REPORT

COD 719

CON A. W. Rengstorf

CON [adamwr@pnw.edu]

OBS H. Hensley, L. Fossel, J. Dong

MEA H. Hensley, L. Fossel, J. Dong

TEL 0.36-m f/11 reflector + CCD

NET NOMAD

BND R

NUM 6

ACK Team 1 - 2000 VJ61

D8846 C2017 06 29.32902 17 24 45.40 -19 56 10.0 15.8 R 719 2017 06 29 07:53:47

D8846 C2017 06 29.34561 17 24 45.01 -19 55 29.3 15.8 R 719 2017 06 29 08:17:41

D8846 C2017 07 12.21403 17 24 45.11 -13 43 28.0 16.1 R 719 2017 07 12 05:08:12

D8846 SC2017 07 12.22771 17 24 45.25 -13 43 10.8 16.3 R 719 2017 07 12 05:27:54

D8846 C2017 07 15.16694 17 25 32.34 -12 49 19.5 16.4 R 719 2017 07 15 04:00:24

D8846 C2017 07 15.18341 17 25 32.53 -12 49 03.3 16.7 R 719 2017 07 15 04:24:07

APPENDIX B: CLOUDY NIGHT RESULTS

Data Collection Strategy/ Methodology:

We strategized the image collection so that as many images as possible could be used for multiple data sets. We started by taking the time-dependent dark images because the first few could be done quickly, and the CCD did not require much cooling. We doubled the exposure each time, and took five images each. The starting exposure time was 5 seconds, and we continued taking pictures until the exposure reached 80 seconds. Then, we proceeded to take the temperature-dependent darks and biases. We started taking pictures at 3° below the ambient temperature, and decreased by 3° each time to reach a final temperature of -10 degrees C.We took five biases and five darks at each temperature. Thus, our final set of time dependent darks doubled as the first set of temperature-dependent darks.

Expected Results:

For the time-dependent darks, we expect the signal to increase linearly with time because in the CCD equation, dark current increases linearly with time. For the temperature-dependent darks, we expect the signal to increase exponentially with temperature.

For the temperature-dependent biases, we expect the signal to remain the same because the exposure time is always zero.

Data Tables:

Darks

Pixel Count vs. Time

Time(s)	Pixel Count	Noise
5	39.28625793	8.542210312
10	81.8257027	9.374951396
20	173.148622	10.72814523
40	374.4290811	13.28186039
80	828.4852683	18.22801156

Pixel Count vs. Temperature

Temperature (degrees Celsius)	Pixel Count	Noise
18.2	828.4852683	18.22801156
15.2	512.623428	14.7911574
12.2	323.2829925	12.6203168
9.2	189.9608427	10.99763018

6.2	112.8366422	9.629267327
3.2	70.00215187	7.34399802
0.2	42.34164797	4.615846541
-2.8	23.72408297	3.197514672
-5.8	14.00186575	2.203315505
-8.8	8.382790384	1.237615789
-11.8	5.26247087	0.68635473

Biases

Pixel Count vs. Temperature

Temperature (degrees Celsius)	Pixel Count	Noise
18.2	1033.766066	7.766838911
15.2	1021.760059	7.512733059
12.2	1014.66007	7.347154483
9.2	1010.04693	7.228327238
6.2	1008.558147	7.112279662
3.2	1006.96138	7.08519446

0.2	1005.950783	7.063755873
-2.8	1005.669032	7.05276601
-5.8	1005.338205	7.049271927
-8.8	1005.232901	7.02700086
-11.8	1005.818731	7.027870327

Data Plots:

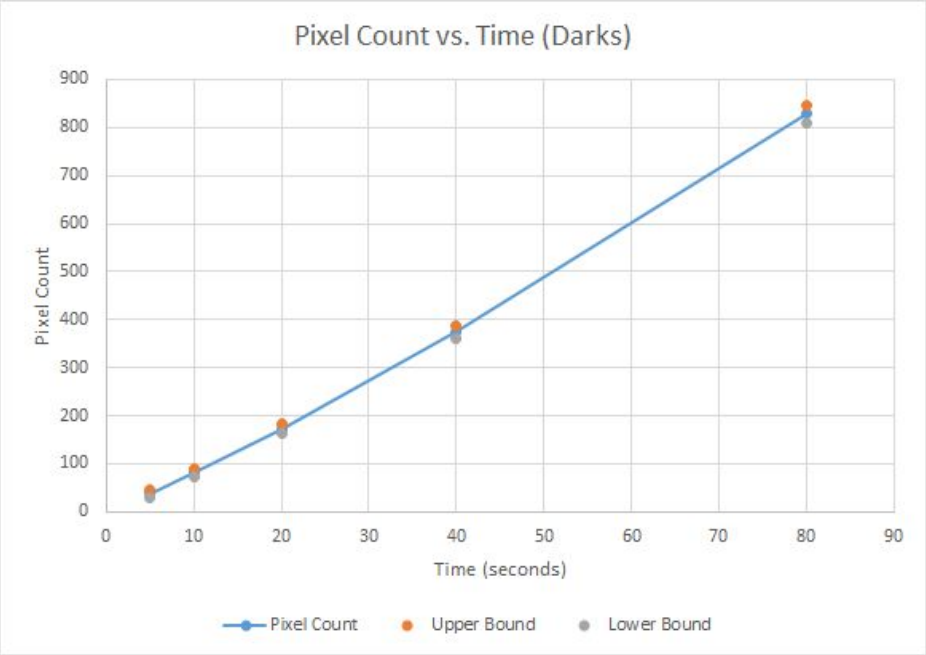

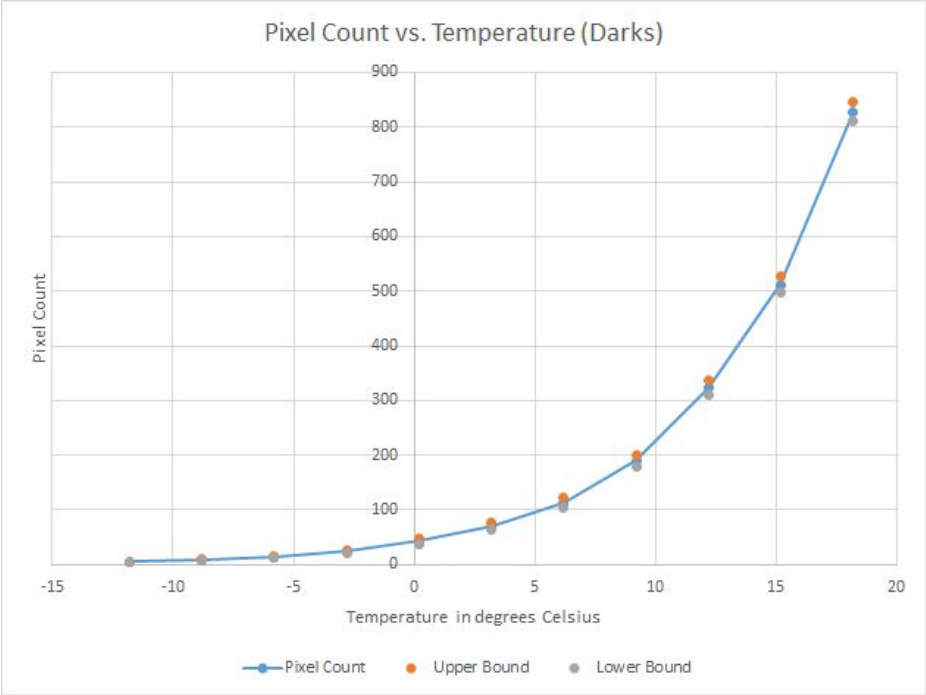
Pixel Count vs. Temperature (Darks)
Pixel Count
900
800
700
600
500
400
300
200
100
0
-15
-10
-5
0
5
10
15
20
Temperature in degrees Celsius
Pixel Count
Upper Bound
Lower Bound

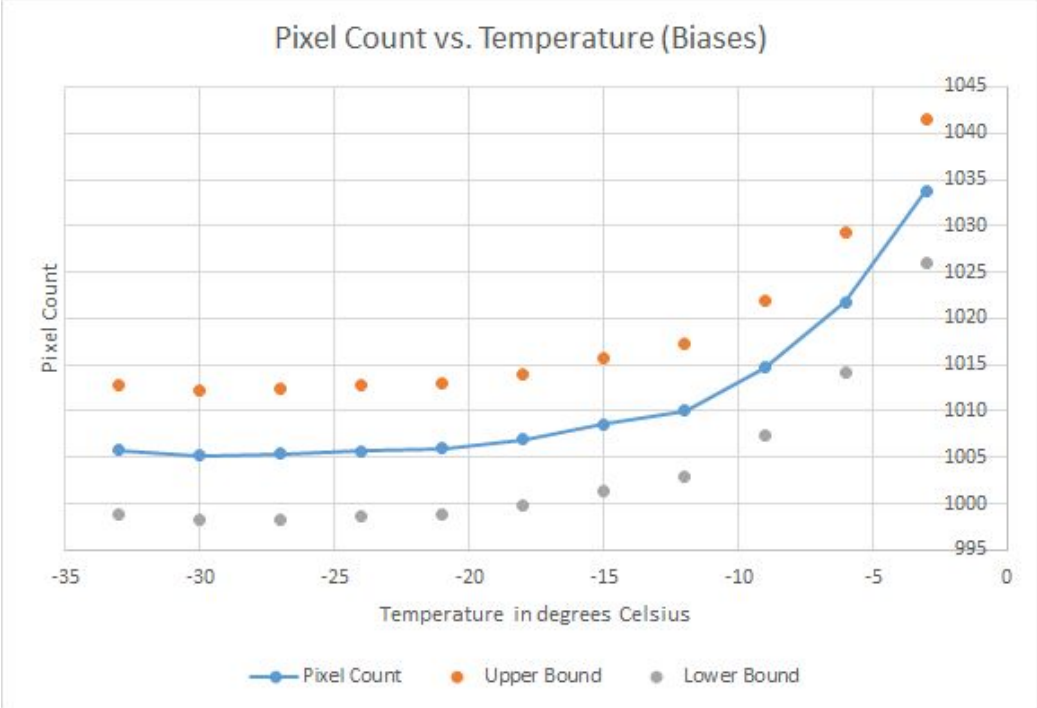
Pixel Count vs. Temperature (Biases)
Pixel Count
1045
1040
1035
1030
1025
1020
1015
1010
1005
1000
995
-35
-30
-25
-20
-15
-10
-5
0
Temperature in degrees Celsius
Pixel Count
Upper Bound
Lower Bound

Analysis:

Darks Time Dependence:

Equation of linear fit line: y = 10.3540817394 x - 22.0911629253

Uncertainty on slope: 0.240364907785

Graph of scatter plot of data points and calculated linear fit line:

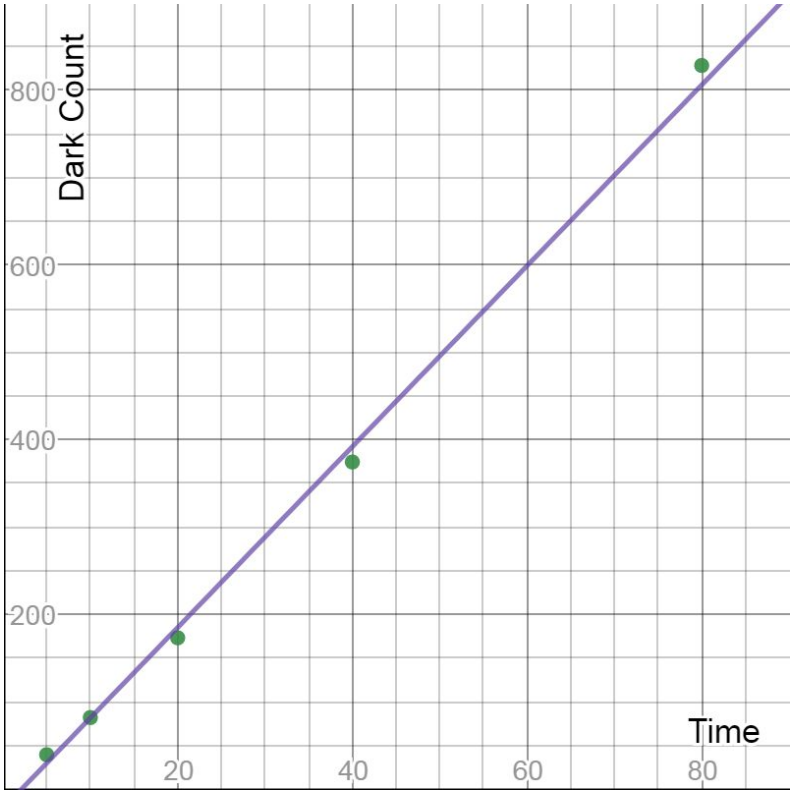

Darks are dependent on time because the uncertainty on the slope is closer to 0 than the slope of the linear fit.

Darks Temperature Dependence:

Equation of exponential fit: y = 1.83667303886e+22 *e^(-12981.5178979 /temp)

Pre-exponential factor: 1.83667303886e+22

Activation Energy of CCD chip: 12981.5178979

Graph of scatter plot of data points and calculated exponential fit:

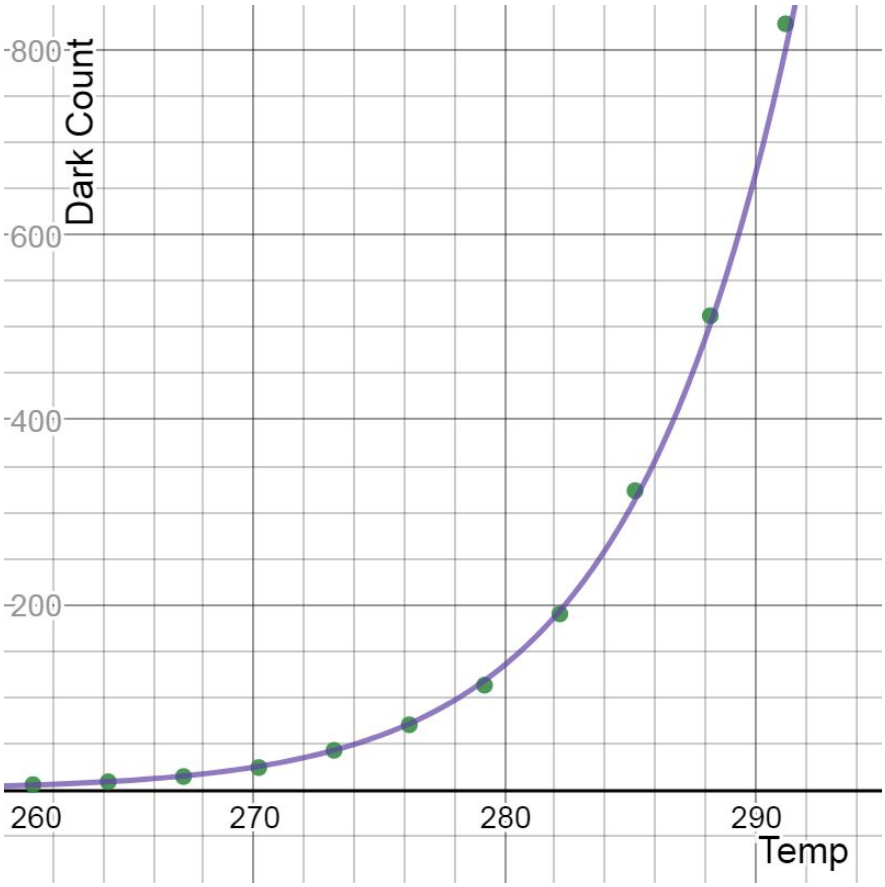

Bias Temperature Dependence:

Equation of linear fit line: y = 0.710929183345 x + 814.738116363

Uncertainty on slope: 0.231861955684

Graph of scatter plot of data points and calculated linear fit line:

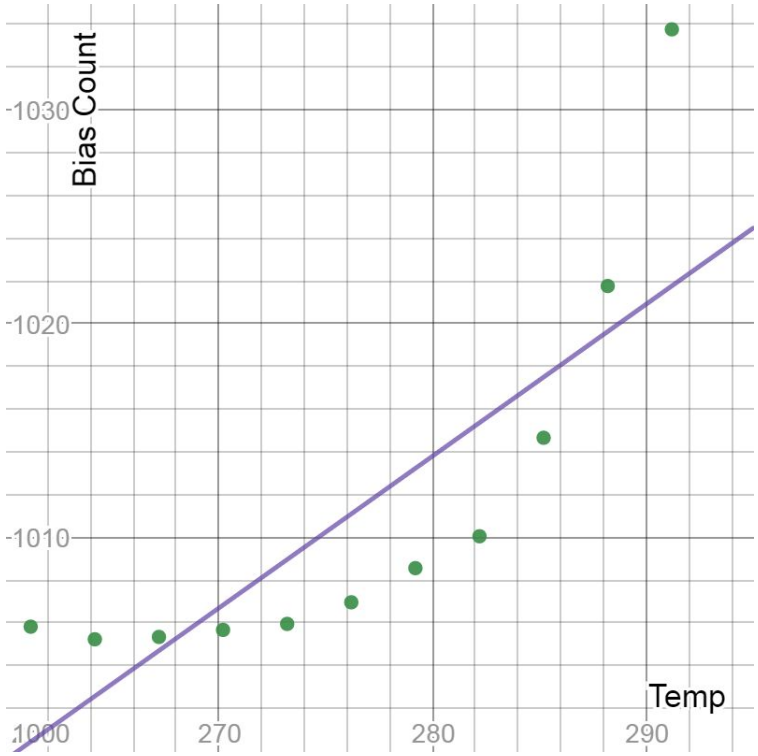

Biases are dependent on temperature because the uncertainty on the slope is closer to 0 than the slope of the linear fit.

Discussion:

By solely analyzing the data plots, the general relationships between the pixel count and time/temperature for the darks/biases can be determined. Also, the plots demonstrate reasonably small noise values. For the dark images with time as the varied parameter, the pixel count increased directly with time. Thus, a linear (y=mx+b) line of fit was used to approximate this relationship. This linear relationship between pixel count and time fits our initial prediction, which was an assumption we made based upon the dark current and time variables within the CCD equation. The dark images with temperature as the varied parameter also fit our initial prediction of an exponential relationship. However, the bias images with temperature dependence did not meet our predictions. We predicted that pixel counts in bias images would

be independent of time due to the fact that bias images have an exposure time of 0 seconds. Yet, our results demonstrate an exponential relationship between pixel count and temperature, which does not make sense because the exposure time is too short for the temperature to affect the pixel count at all. The exact reason for this discrepancy is unclear, but it could possibly be attributed to some of the dark image getting caught in the bias. Although the linear regression on the biases predicts a direct relationship to temperature, we cannot assume that it is correct because 1) the linear fit is not entirely appropriate for the data, which appears very nonlinear, and 2) there might have been some error in the bias images themselves.

Conclusion:

Overall, our data collection procedures for this experiment were sufficient to get all of the required data for each image and varying parameter. After a careful analysis of our data, we came to the conclusion that our experiment was successful in showing that dark images with varied time and temperature show some levels of dependence. However, our data suggested that pixel counts in biases might be dependent on temperature.